



Response Mechanism of Offshore Wind Turbine Single-Cell Foundation Under Long-Term wind and Wave Action

Xiaofang Jia^{1,a}, Bo Wang^{1,b}, Chengshun Xu^{1,c*}, Shuo Li^{1,d}, Kaiyuan Liu^{2,e}

¹Key Laboratory of Urban and Engineering Safety and Disaster Reduction, Ministry of Education, Beijing University of Technology, Beijing 100124, China

² China Three Gorges Corporation Research Institute of Science and Technology, Beijing 100000, China

^a 13994267641@163.com; ^b wb202489003@gmail.com;

^{c*} Corresponding author: xcs_2017@163.com;

^d 1037770460@qq.com; ^e liukygeo@163.com

Abstract. The single-cylinder foundation for offshore wind power has significant application potential in China's wind power industry, particularly for deep-water regions, due to its ease of installation and excellent resistance to overturning. This paper investigates the response characteristics of the soil surrounding the barrel foundation subjected to combined wind and wave loading through numerical simulations. Results show that soil settlement gradually decreases with increasing horizontal distance from the foundation and also declines with increasing vertical depth, rapidly attenuating beyond a specific distance from the cylinder. The pore pressure distribution is positively correlated with the burial depth of the cylinder and increases significantly under cyclic loading. Horizontally, pore pressure decreases with increasing lateral distance from the cylinder, forming an elliptical high-pressure zone at the cylinder base, which reduces the shear strength of the surrounding soil. The soil around the suction cylinder foundation primarily undergoes asymmetric plastic deformation, leading to tilt-rotation shear damage, while the foundation itself remains undamaged.

Keywords: combined wind and wave forces; numerical simulation; long-term cyclic loading; single-pile foundation; dynamic behavior

1 Introduction

China has a long coastline and abundant wind energy resources, and its offshore wind power industry^[1] is rapidly expanding from shallow to deeper waters. Suction cylinder foundations (<45m sea area^[2]) are widely used due to their easy installation and strong resistance to overturning. In actual projects, suction cylinder foundations must withstand horizontal loads induced by dynamic factors such as earthquakes, offshore wind, and waves. These loads can cause foundation tilt, potentially affecting the long-term performance of the structure. In recent years, most studies have focused on the dynamic

response and bearing characteristics of suction cylinder foundations in sand and clay layers under short-term cyclic loading. However, limited research has systematically investigated the evolution of soil properties and failure mechanisms under long-term combined wind and wave loading in liquefiable sites. Existing analytical frameworks for these processes remain incomplete and require urgent refinement and further exploration.

Many scholars have conducted in-depth studies on the force characteristics of cylinder foundations under dynamic loads. In theoretical analyses, Changka ^[3] et al. compared the effectiveness of the full-coupling method, stress superposition method, and fatigue damage superposition method in evaluating the fatigue damage of cylinder foundations. This research provided theoretical support for understanding the long-term mechanical response of cylinder foundations under cyclic loading. To further validate these theoretical analyses, researchers conducted numerical simulations and scaled-down tests to examine the soil-structure interaction mechanisms and key influencing factors. In numerical simulations, Yang Chunbao ^[4], Yuan Minghui ^[5], Sun Xiyuan ^[6], and Cheng ^[7] investigated the dynamic behavior of suction cylinder foundations in saturated sandy soil and soft clay by constructing refined finite element models. In experimental studies, Luo Lunbo ^[8] et al. investigated the horizontal ultimate bearing capacity and cyclic loading response of suction cylinder foundations in sandy soil using 1-g indoor tests. Li Chi ^[9] et al. revealed the response mechanism of single-cylinder foundations under combined dynamic and static loads through cyclic triaxial tests in soft clay. Jiao Bintian ^[10], Lu Xiaobing ^[11], Jeong Y H ^[12], and others investigated the mechanical characteristics of barrel foundations under horizontal loads using centrifuge tests. Additionally, combining numerical simulations and tests provides a more comprehensive assessment of the dynamic response of the barrel foundation. Lian J ^[13] et al. conducted a series of single-gravity model tests, which showed that under unidirectional cyclic loading, sandy soil tends to densify inside the barrel, while localized weakening occurs outside the barrel. Zhu Bin ^[14] et al. and Achmus ^[15] et al. combined model tests with numerical simulations to systematically analyze the horizontal bearing capacity of suction drum foundations. Overall, a comprehensive research framework combining theoretical analysis, numerical simulation, and physical testing has gradually emerged. In particular, multi-scale joint analysis has been increasingly used to investigate the anti-tilting capacity and long-term performance of suction cylinder foundations. This combined approach has significantly enhanced understanding of the dynamic evolution mechanisms of suction cylinder foundations under cyclic loading. As research progresses, scholars have increasingly focused on the application of cylinder foundations in liquefiable sandy soil strata. Studies indicate that the strength and deformation characteristics of soil in liquefied sites are significantly influenced by loading, which has a crucial impact on cylinder foundation stability ^[16-19]. However, systematic research on the failure modes and long-term dynamic response evolution of suction cylinder foundations under liquefied site conditions remains limited. In particular, the complex soil-structure interactions under combined wind and wave loading have not yet been fully clarified.

The study of the response mechanism of offshore wind turbine foundations under long-term cyclic loading is crucial to their stability and service life. However, there is

a gap in the current research, particularly in the analysis of the dynamic response of liquefiable sites, where research on turbine foundations remains insufficient. This paper focuses on the response mechanism of the offshore wind turbine single-cylinder foundation under the combined effects of wind and waves. Using numerical simulations on the OpenSees finite element platform, we analyze core parameters such as soil settlement and superporous pressure ratio in liquefiable sites under long-term wind and wave loading conditions, aiming to reveal the patterns of site response and foundation failure modes.

2 Validation of Numerical Model for Single-Cylinder Foundation Structures of Offshore Wind Turbines Based on Shaker Tests

2.1 Overview of Shaker Testing

The tests were conducted on a seismic vibration table at the Key Laboratory of Urban and Engineering Safety and Disaster Reduction, Ministry of Education, Beijing Institute of Technology. The model structure prototype used in the test was based on a real offshore wind farm project, and the GW171-6.45 MW turbine was chosen for testing with a 1:70 scale ratio.(Table 1)

This test requires the preparation of a model foundation consisting of an upper 0.42 m thick homogeneous saturated sand layer and a lower 0.73 m thick dense sand layer. The water level line and the upstream boundary of the saturated sand layer are maintained consistently.

This study investigates the dynamic response of wind power structures under the combined effects of wind, waves, and earthquakes. A specially customized mechanism is used to apply constant wind and wave loads with a peak value of 20 N and a frequency of 0.1 Hz.(Fig. 1)

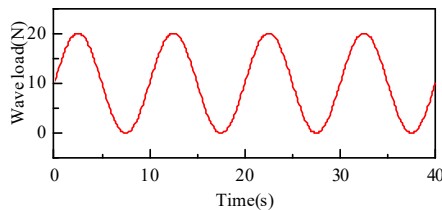


Fig. 1. Time history of constant wind and wave loads

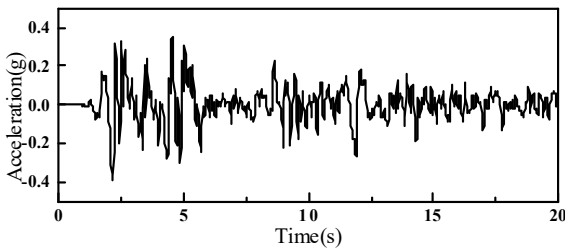
Table 1. Test model fan structural parameters

Actual structure	Test structure	Parametric
Upper fan	Steel Mass Blocks	Diameter 120mm, Height 35mm, Mass 3kg

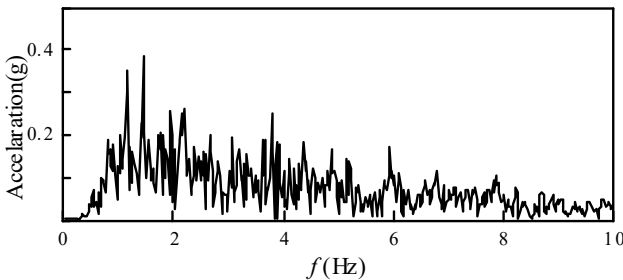
Turbine	Steel pipe	Outer diameter 100mm, wall thickness 1mm, length 1200mm
Transition section of cylinder foundation	Two sections of welded steel pipe	Diameter of the upper part is 100mm, diameter of the lower part is 140mm, thickness of the cylinder wall is 1mm
Tube cover	Cylinder	Diameter 340mm, height 5mm
Lowermost part of the cylinder foundation	Traffic circle	Diameter 340mm, height 340mm, wall thickness 1mm

Note: Four triangular support plates (120 mm × 100 mm × 1 mm) are welded at the bottom of the transition section of the cylinder foundation. The cylinder cover is equipped with two exhaust valves, each with a 30 mm diameter. Additionally, the foundation and the tower are rigidly connected.

The EL Centro seismic record was selected as the input ground motion for this shaker test to determine the dynamic characteristics of the model system, including its natural frequency and damping ratio, with a peak acceleration of 0.35 g. The corresponding acceleration time-history curves and Fourier spectra are shown in **Fig. 2**.



(a) EL Centro acceleration time-history



(b) EL Centro Fourier spectrum

Fig. 2. Input acceleration time-history and Fourier spectrum of ground motion

The test was conducted in a container with dimensions 2.3 m × 1.2 m × 1.5 m (L × W × H). The sensor layout of the test model is shown in **Fig. 3**.

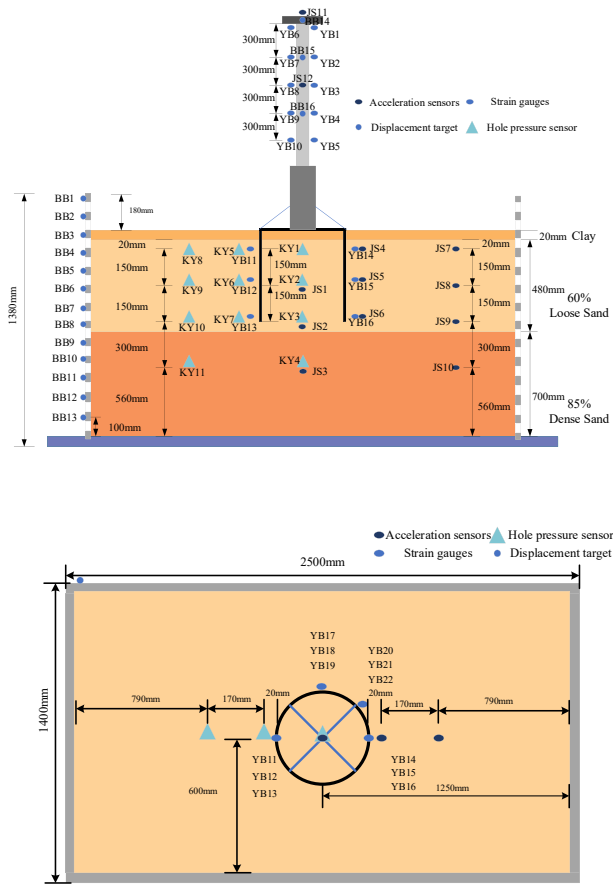


Fig. 3. Layout of experimental sensors

2.2 Finite Element Numerical Simulation

Table 2. Numerical model turbine structural parameters

Physical quantity	Modelling
Tower length/m	1.2
Tower wall thickness/mm	1
Tower diameter/m	0.1
Length of transition section/m	0.65
Transition section wall thickness/mm	1
Diameter of transition section/m	0.14
Cylinder base length/m	0.34
Cylinder base wall thickness/mm	1
Cylinder base diameter/m	0.34

This study utilizes the OpenSees finite element platform, selected primarily for its strong capabilities in simulating nonlinear soil-structure interactions. OpenSees offers well-established methods for describing multi-field coupling processes, including pore pressure, liquefaction, and intrinsic soil nonlinearity. Moreover, it efficiently captures soil deformation and excess pore pressure evolution under cyclic loading conditions. Based on the above test, the model similarity ratio was set to 1:70. The wind turbine structural dimensions are consistent with the test model. The specific parameters are listed in **Table 2**. Both the barrel foundation and tower are made of Q235 steel. The superstructure is rigidly connected to the tower, which in turn is rigidly connected to the barrel foundation.

The foundation and tower are modeled using the dispBeamColumn element, while the superstructure is modeled using the SSPbrick element. The Steel02 material model is used to simulate the mechanical behavior of the steel tube, and the structural material parameters are listed in **Table 3**.

Table 3. Material parameters of steel

Material name	Modulus of elasticity (kPa)	Yield strength (kPa)	Isotropic strengthening parameters	Kinematic reinforcement modulus (kPa)
Steel cylinder	2.1×10^8	235000	0.02	1.6129×10^6

The pile nodes were connected to the soil nodes using modified ASDimplex zero-length elements. Horizontal and vertical displacements were constrained at the model bottom, while the lateral boundaries at the bottom and around the perimeter were set as undrained. To simulate shear boundaries, nodes at the same depth on opposite sides of the model were coupled using the equalDOF command. The site was modeled using SSPbrickUP elements, with soil parameters listed in **Table 4**.

Table 4. Soil unit parameters

Unit parameter	Clay layer	Saturated sandy soil
Horizontal gravitational acceleration $/(m/s^2)$	0.0	0.0
Vertical gravitational acceleration $/(m/s^2)$	-9.81	-9.81
Liquid phase undrained bulk modulus /kPa	2.2×10^6	2.2×10^6
Space pressure field stabilisation parameters	6.0×10^{-5}	6.0×10^{-5}
X-permeability coefficient $/(m/s)$	1.0×10^{-10}	1.0×10^{-6}
Y-permeability coefficient $/(m/s)$	1.0×10^{-10}	1.0×10^{-6}
Z-permeability coefficient $/(m/s)$	1.0×10^{-10}	1.0×10^{-6}

For the selection of soil elements, the PDMY02 multi-yield surface plasticity model and the PIMY multi-yield surface elasto-plastic model were selected to capture the complex dynamic behavior and liquefaction potential of saturated sand and clay at the site. These two models have been extensively validated in numerous studies on the dynamic response of liquefiable sites and are capable of accurately simulating the nonlinear dynamic behavior and liquefaction evolution of sand and clay. They provide a reliable basis for evaluating soil deformation and pore pressure accumulation under long-term combined wind and wave loading. The soil material parameters are listed in **Table 5**.

A numerical model of an offshore wind turbine single-cylinder foundation-structure system on a saturated sandy soil site was developed. The EL Centro ground motion was used as the primary seismic input, with a peak acceleration of 0.35 g. Additionally, a sinusoidal wind-wave load with an amplitude of 20 N was applied 1 m below the turbine top. The dynamic nonlinear characteristics and energy dissipation capacity of the soil were modeled using Rayleigh damping, with a damping ratio of 0.03^[20].

Table 5. Soil principal structural parameters

Parametric	Saturated sandy soil	Parametric	Confined sand layer
Mass density $\rho(\text{kg}/\text{m}^3)$	1516	Mass density $\rho(\text{kg}/\text{m}^3)$	1594
Reference shear modulus Gr(kPa)	27500	Reference shear modulus Gr(kPa)	35000
Reference bulk modulus Br(kPa)	60000	Reference bulk modulus Br(kPa)	68750
Friction angle	35	Friction angle	37.5
Octahedral peak shear strain γ_{max}	101	Octahedral peak shear strain γ_{max}	101
Reference peripheral pressure (kPa)	0.5	Reference peripheral pressure (kPa)	0.5
Shrinkage parameter c_1	0.028	Shrinkage parameter c_1	0.008
Shrinkage parameter c_2	0.05	Shrinkage parameter c_2	0.0
Shear expansion parameters d_1	0.1	Shear expansion parameters d_1	0.4
Shear expansion parameters d_2	0.05	Shear expansion parameters d_2	0.0
Number of yield surfaces	20	Number of yield surfaces	20
Standard atmospheric pressure constant (kPa)	101	Standard atmospheric pressure constant (kPa)	101

The dynamic response of the offshore wind turbine single-cylinder foundation-structure under combined wind, wave, and seismic loads was obtained through numerical

simulations. To ensure the accuracy and applicability of the numerical model, the material parameters and site conditions were derived from the geological survey report of the actual project. These parameters were further supplemented and refined using typical saturated sand and dense sand parameters reported in the literature to enhance their representativeness and engineering relevance. In addition, the loading amplitude and frequency of wind and wave forces were determined by integrating existing wind farm monitoring data with findings from relevant studies, ensuring that the model realistically reflects the long-term service environment of the suction cylinder foundation under combined wind and wave loading.

2.3 Validation of Model Accuracy

This study focuses on the offshore wind turbine single-cylinder foundation. A computational model was developed based on a large-scale shaker test of a single-cylinder foundation to validate numerical simulations through comparison.

Fig. 4 presents the numerical simulation results of the variation in excess pore pressure ratio over time at different site depths, compared with experimentally measured data. The numerical simulation results at each measurement point generally exhibit trends consistent with the test measurements. The excess pore pressure ratio fluctuates significantly and rises rapidly in the initial stage of seismic loading, before stabilizing in the middle and late stages, reflecting the typical behavior of saturated sandy soils during liquefaction. Although some discrepancies exist in local peak values, likely due to sand distribution non-uniformity during testing and sensor sensitivity limitations, the high overall consistency between the numerical simulation and measured data confirms that the proposed numerical model accurately captures the dynamic evolution of pore water pressure. This validation further demonstrates the model's effectiveness and accuracy in representing pore pressure behavior during site liquefaction.

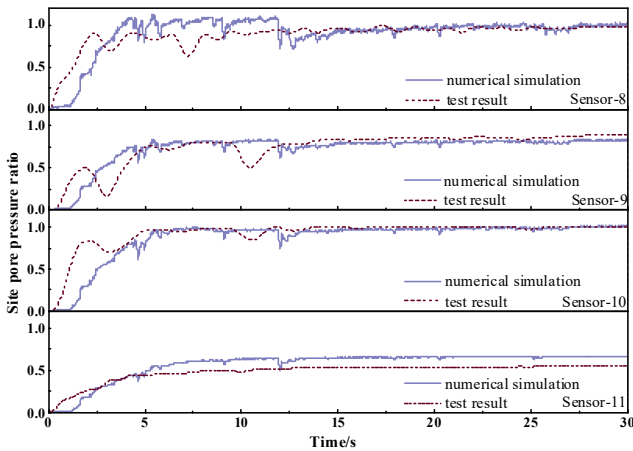


Fig. 4. Comparison of pore pressure ratio between experimental and numerical results for cylindrical sites

Fig. 5 and **Fig. 6** present the numerical simulation and experimentally measured acceleration time histories at different site depths and along the structure's height, respectively. As shown in the figures, the numerical simulation results at various measurement points exhibit good agreement with the experimentally measured values, confirming the high accuracy of the developed finite element model.

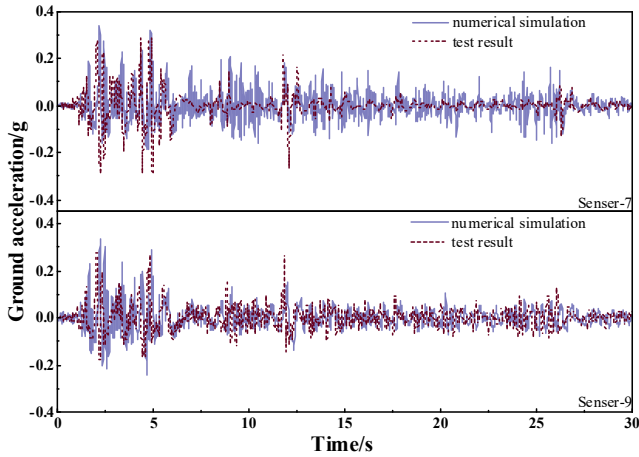


Fig. 5. Comparison of acceleration between experimental and numerical results for a cylindrical foundation site

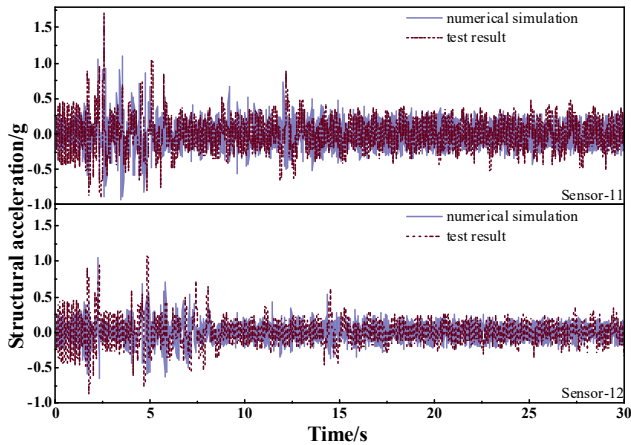


Fig. 6. Comparison of acceleration between experimental and numerical results for a cylindrical base structure

In summary, the numerical simulation results for each response are largely consistent with the test results. Therefore, the three-dimensional finite element model developed on the OpenSeesMP platform effectively replicates the large-scale shaking table test of a single-cylinder foundation. Using this modeling approach, numerical simulations can be conducted for saturated sandy soil in liquefiable sites under long-term cyclic wind and wave loading. Additionally, key parameters such as soil settlement and excess pore pressure ratio can be further investigated.

3 Numerical Simulation of the Dynamic Response of a Single-Cylinder Foundation-Structure for Offshore Wind Power at an Actual Site

3.1 Introduction to Numerical Modelling

The actual site consists of a 1.4 m clay layer, a 33.6 m saturated sand layer, and a 49 m dense sand layer from top to bottom. The water table is set at a depth of 1.4 m. The superstructure of the test model has a mass of 500 tonnes. The tower consists of two sections: the upper section is 110.6 m long, with an external diameter of 7 m and a wall thickness of 0.07 m. The lower section, serving as a transition segment, has a length of 18.9 m, an external diameter of 9.8 m, and a wall thickness of 0.07 m. The cylinder cover is a cylindrical structure with a diameter of 23.8 m and a height of 0.35 m. The cylinder body is an annular structure with an external diameter of 23.8 m, a height of 23.8 m, and a wall thickness of 0.07 m. The foundation is embedded 23.8 m into the soil, with a wall thickness of 0.07 m. The tube foundation and tower are made of Q235 steel. The superstructure is rigidly connected to the tower and tower foundation. The numerical model diagram is shown in **Fig. 7**.

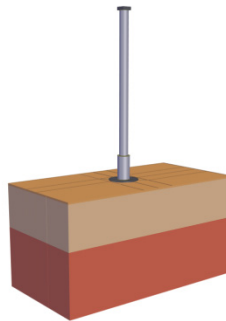


Fig. 7. Finite Element Model Diagram

Studies indicate that boundary effects in numerical simulations become negligible when the site size exceeds 15 times the cylinder diameter. Based on this finding, a site with dimensions of 714 m \times 714 m \times 84 m was selected for the simulation, where the

length in the direction of ground vibration application is 30 times the cylinder diameter (30D). Thus, boundary effects are assumed to be negligible in this simulation.

In accordance with the objectives of this experimental study, the applied horizontal load comprises combined wind and wave forces, which are considered equivalent to horizontal cyclic loads. Cuéllar P. [21] demonstrated that within a horizontal cyclic load frequency range of 0.01 to 0.2 Hz, frequency variations have a negligible effect on induced excess pore water pressure. Additionally, Naggar M.H.E. [22] suggested that a frequency range of 0 to 1 Hz is appropriate for offshore environmental loads. Based on this, a loaded displacement amplitude of 0.5 m at a frequency of 0.2 Hz is selected as the equivalent long-term wind and wave load for the numerical model. This selection is supported by existing studies, such as the strain superposition method based on the damage relationship, which was adopted by Lin S.S. [23] to predict the cumulative horizontal displacement of piles under variable-amplitude cyclic loading. However, their tests were limited to 50 cycles, making it difficult to fully capture the bearing characteristics under long-term cyclic loading. Li Dayong et al. [24] increased the number of loading cycles to 1000 to better simulate long-term cyclic loading, achieving a good fit between experimental and predicted results. Moreover, Chong et al. [25-26] employed explicit hybrid analysis to study the cumulative horizontal displacement evolution of offshore wind turbine monopile and gravity foundations under cyclic loading. They observed that significant cumulative deformation in pile foundations primarily occurs in the early stage of cyclic loading, particularly when the number of loading cycles (N) is fewer than 100. Therefore, a total of 200 cyclic loads are applied in this study to better simulate long-term wind and wave loading conditions. (Fig. 8)

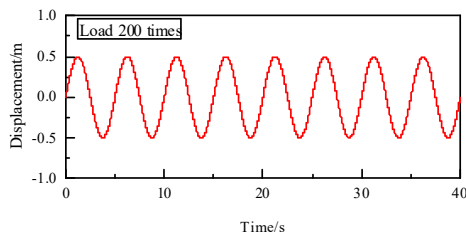


Fig. 8. Spectrogram of long-term wind and wave loads

A three-dimensional finite element model of a large-scale offshore wind turbine single-cylinder foundation was developed using the OpenSeesMP computational platform, incorporating the combined effects of wind, waves, and currents. Horizontal and vertical displacements were constrained at the model bottom, while the bottom and surrounding side boundaries were set as undrained. To simulate shear boundaries, nodes at the same depth on opposite sides of the model were coupled using the equalDOF command. The site was modeled using SSPbrickUP elements, with material parameters for steel and soil consistent with the experimental model. Clay soil was simulated using the PIMY multi-yield surface elastic-plastic model, while saturated sand was modeled using the PDMY02 multi-yield surface plasticity model. The soil unit parameters are listed in Table 6.

Table 6. Soil principal structural parameters

Parametric	Saturated sandy soil	Parametric	Confined sand layer
Mass density ρ (kg/m ³)	2000	Mass density ρ (kg/m ³)	2200
Reference shear modulus Gr(kPa)	110000	Reference shear modulus Gr(kPa)	140000
Reference bulk modulus Br(kPa)	240000	Reference bulk modulus Br(kPa)	275000
Friction angle	35	Friction angle	37.5
Octahedral peak shear strain γ_{max}	101	Octahedral peak shear strain γ_{max}	101
Reference peripheral pressure (kPa)	0.5	Reference peripheral pressure (kPa)	0.5
Shrinkage parameter c_1	0.028	Shrinkage parameter c_1	0.008
Shrinkage parameter c_2	0.05	Shrinkage parameter c_2	0.0
Shear expansion parameters d_1	0.1	Shear expansion parameters d_1	0.4
Shear expansion parameters d_2	0.05	Shear expansion parameters d_2	0.0
Number of yield surfaces	20	Number of yield surfaces	20
Standard atmospheric pressure constant (kPa)	101	Standard atmospheric pressure constant (kPa)	101

3.2 Numerical Simulation of Long-Term Wind and Wave Loading Effects

1). Variation of Soil Settlement Depth Around the Cylinder

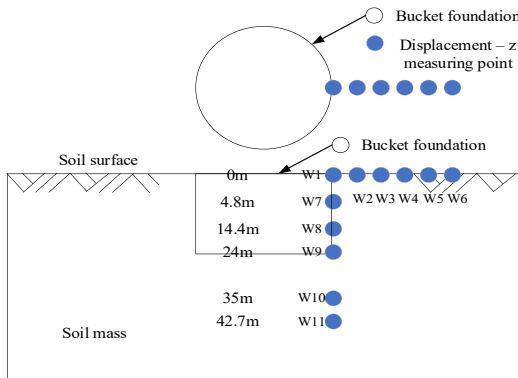


Fig. 9. Schematic of Soil Displacement Measurement Points Around the Cylinder

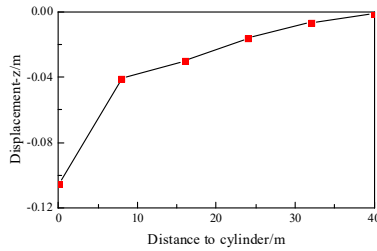


Fig. 10. Backbone Curve of Peak Settlement Displacement at the Cylinder Periphery

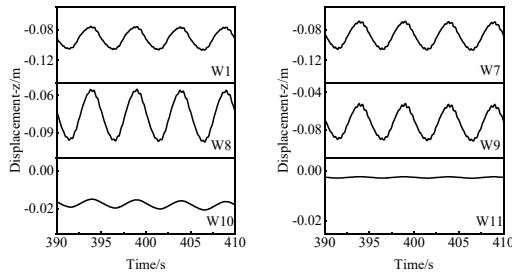


Fig. 11. Longitudinal Displacement and Settlement at the Cylinder Side

Using the right edge of the cylinder as the reference point, measurement points are placed horizontally at 8 m intervals, and six vertical depths are selected: 0 m, 4.8 m, 14.4 m, 24 m, 35 m, and 42.7 m. The measurement points are labeled W1 to W11. Based on the analysis of the full-time data, the time period during which the system response stabilizes is selected to effectively eliminate initial transient disturbances. The chosen time range is 390–410 s. (Fig. 9)

Fig. 10 shows the backbone curve of the peak soil surface displacement subsidence around the cylinder. The subsidence peaks at six measurement points, spaced 8 m radially on the cylinder side, exhibit a marked attenuation trend. The surface settlement approaches zero at a distance of 40 m from the cylinder's edge (approximately 1.7 times the cylinder's diameter), indicating that the subsidence impact follows the typical spatial attenuation pattern. Fig. 11 shows the fluctuation amplitude of soil settlement at different depths along the side of the cylinder after stabilization. As depth increases, soil settlement exhibits sinusoidal fluctuations with decreasing amplitude, becoming negligible at approximately 42.7 m (about 2.1 times the cylinder diameter). This phenomenon corresponds to the spatial distribution of pore pressure beneath the cylinder, further confirming that settlement effects are primarily concentrated in the near-field region surrounding the cylinder. Notably, the soil under cyclic loading exhibits a typical fatigue response, characterized by gradual stiffness degradation and continuous accumulation of plastic deformation during repeated loading-unloading cycles. Consequently, settlement significantly increases in later cycles at the same stress level, a phenomenon particularly pronounced in shallow soil layers (0–14.4 m).

Based on the model data, the maximum soil subsidence depth around the cylinder is 0.16 meters. The horizontal influence radius extends to approximately 1.7 times the

cylinder's diameter, while the vertical depth of influence reaches 2.1 times the diameter. **Fig. 12** provides a top view of the subsidence depth distribution, clearly showing the spatial extent of the maximum subsidence area.

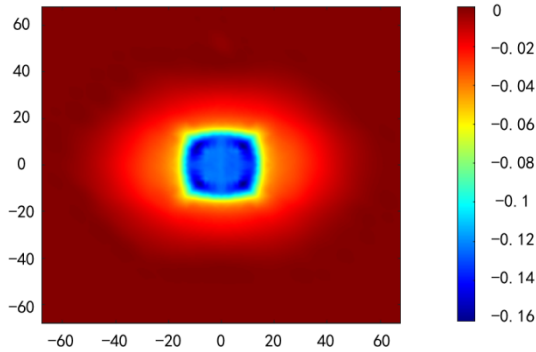


Fig. 12. Distribution of maximum soil subsidence displacement around the cylinder

2). Analysis of Soil Pore Pressure Changes

For the in-depth numerical analysis of pore pressure distribution around the cylinder, the soil is classified based on distance from the cylinder's center. The zones are: Zone I (inside the cylinder, at the center), Zone II (at the cylinder-soil interface), and Zone III (free-field, 60 m from the center). Four depth levels are selected for analysis: 4.8 m, 9.6 m, 14.4 m, and 29.5 m, as shown in **Fig. 13**.

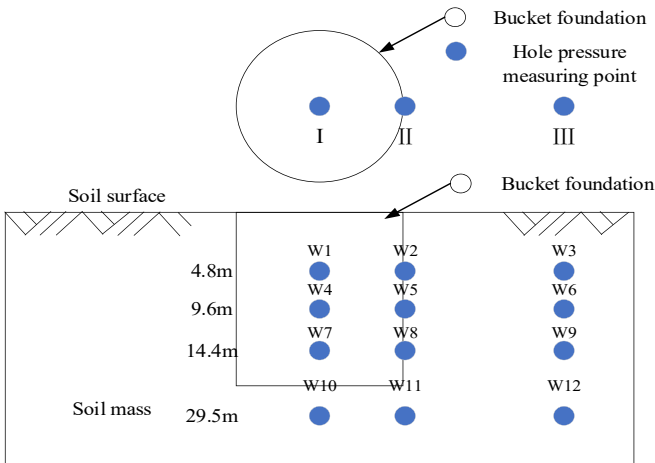


Fig. 13. Schematic diagram of borehole pressure measurement points in the soil around the cylinder

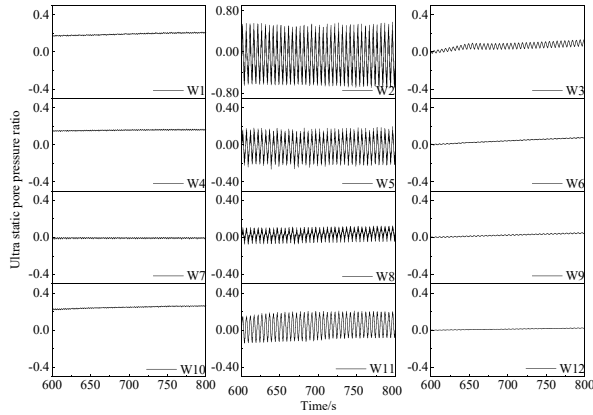
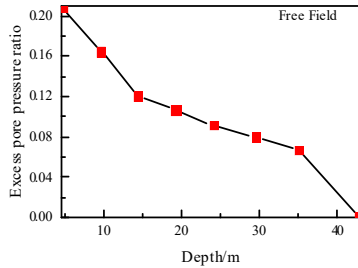
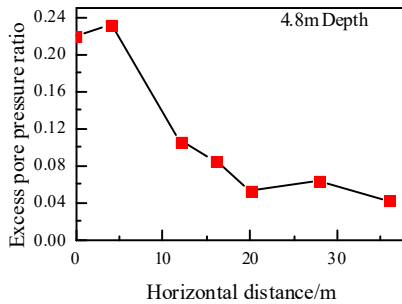


Fig. 14. Variation of the soil overpressure ratio with depth at different locations



(a) Distribution of free-field superporous pressure ratios along depth



(b) Distribution of superporous pressure ratio along the horizontal direction

Fig. 15. Depth distribution of superhole pressure ratio

Based on the model data analysis, the superhole pressure ratio was introduced for numerical calculations, and the ratio n was determined using Eq^[27]

$$n = \frac{u}{\sigma_v}$$

Where: u represents the superporous pressure, σ_v represents the effective vertical stress, which is the sum of the self-gravity stress and the additional stress from the applied upper loads.

Fig. 14 presents a comparison of the superporous pressure ratios in different zones and depths around the cylinder. In the first three depths, when comparing zone I with zones II and III, the non-drainage condition of the cylinder causes a cumulative increase in the superporous pressure ratio, resulting in a smaller fluctuation amplitude. In zone II, where pore water is expelled from the cylinder wall, the fluctuation amplitude of the superporous pressure ratio is largest, with the highest value observed. In zone III (the free field), the superporous pressure ratio is clearly lower than in zone I, but still shows a slight fluctuation, indicating that cyclic loading in the free field also exerts some influence. As the depth increases, reaching the region beneath the cylinder, an ellipsoidal high-pressure stress zone forms at the bottom. This causes a reversal in the superporous pressure ratio, with the value at 29.5 m being larger than at 14.4 m. **Fig. 15** shows that under free-field conditions, the soil superporous pressure ratio tends to decrease with depth and decreases as the horizontal distance from the cylinder foundation increases, with only minor fluctuations in some areas.

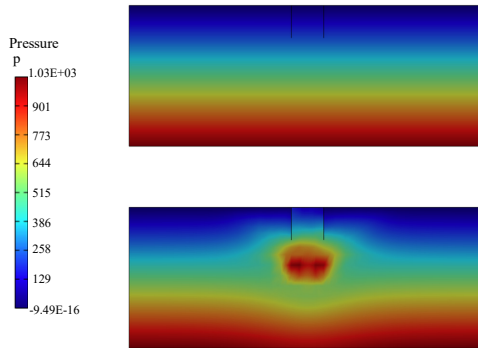


Fig. 16. Horizontal distribution of pore water pressure around the cylinder

The illustration above shows the horizontal mid-axis profile of the soil around the cylinder, with a focus on the pore water pressure distribution under cyclic loading. The figure clearly shows a significant anomaly in pore water pressure beneath the cylinder—a high-pressure ellipsoidal zone extends from a depth of 24m (1D, D is the cylinder diameter) to 58m (2.4D) along the axis, with a horizontal radius of influence reaching 40m (1.7D). The large-diameter single-cylinder foundation of offshore wind turbines exhibits rotational shear damage under horizontal loading. The soil near the end of the cylinder deforms significantly, increasing pressure and pore water pressure, which decreases the soil's bearing capacity. This phenomenon indicates that when the soil at the cylinder's end undergoes dense subsidence, soil damage can occur, preventing effective pore water discharge and potentially threatening the stability of the single-cylinder foundation. (**Fig. 16**)

4 Analysis of Failure Modes in Single-Cylinder Foundations

Under long-term cyclic loading from waves and wind, transient pore pressures generated during the cylinder-soil interaction undergo cycles of buildup and dissipation, resulting in continuous consolidation and densification of the soil surrounding the cylinder. This study finds that the cylinder foundation exhibits progressive damage under cyclic loading. Results indicate that asymmetric cumulative plastic deformation, driven by loading direction, creates a pronounced inverted conical settlement pattern around the cylinder. Subsidence depth varies significantly on both axial sides, and an additional conical subsidence zone forms beneath the cylinder near the rotation point. The soil at the cylinder base experiences rotation and tilting, leading to progressive shear damage. The expansion of this damage surface aligns with the development of a plastic shear slip zone. As shown in **Fig. 17**, the cylinder foundation ultimately exhibits rotational shear deformation dominated by tilting under prolonged cyclic loading.

The primary failure mode of the single-cylinder foundation is characterized by overall upward pullout damage, with its pullout capacity largely dependent on cylinder-side frictional resistance. Due to its closed structure, the cylinder foundation exhibits a more concentrated failure zone and a lower rotation center, providing higher overall stiffness and greater resistance to overturning. Earth pressure has a limited contribution to the failure process, but the cylinder-soil interaction significantly enhances foundation stability, improving performance under prolonged cyclic loading from wind, waves, and currents, as well as extreme conditions. In summary, single-cylinder foundations offer higher stiffness and improved resistance to horizontal loads, making them more suitable for offshore wind power and other extreme operational environments.

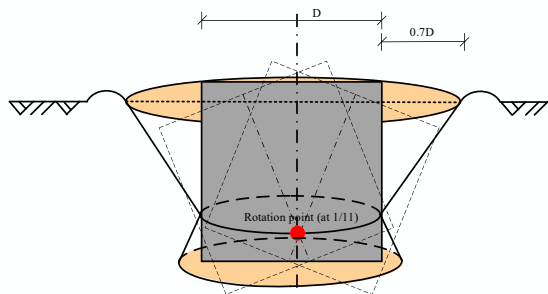


Fig. 17. Simplified model of soil deformation around the cylinder

5 Conclusion and Prospect

This study systematically analyzes the settlement and pore pressure distribution around the suction cylinder conduit rack foundation in both horizontal and vertical directions. These findings provide essential insights into the site response and failure mechanisms of suction cylinder foundations under long-term cyclic loading.

1. The settlement depth of the soil around the cylinder foundation decreases progressively with increasing horizontal distance from the cylinder and with increasing vertical depth. The primary settlement influence area is defined as a roughly rectangular zone, beyond which the settlement effect attenuates rapidly. This feature clearly illustrates the spatial distribution pattern of soil settlement around the suction cylinder foundation, providing important support for revising the traditional assumption of symmetric settlement.

2. The superstatic pore pressure ratios of the soil around the cylinder varied significantly with depth and location. In zone I (inside the cylinder), the superstatic pore pressure ratio remained stable with minor fluctuations, as the soil inside the cylinder is undrained. In contrast, the pore pressure ratio in zone II (at the side of the cylinder) exhibited the largest fluctuations, reflecting the significant effects of cyclic loading. In zone III (the free field), the pore pressure ratio was lower than in zone I but still exhibited small fluctuations, showing the effect of drainage from the cylinder wall. As the depth increases beneath the cylinder, the superstatic pore pressure ratio reverses and increases, forming an ellipsoidal high-pressure zone at the bottom, which suggests that pore pressure distribution under the cylinder foundation is depth-dependent.

3. Under cyclic loading, the failure mechanism of single-cylinder foundations is primarily governed by asymmetric plastic deformation, characterized by tilt-rotation shear damage. The pull-out bearing capacity is mainly dependent on the lateral frictional resistance of the cylinder. The soil subsidence around the cylinder comprises two distinct zones: an inverted conical subsidence area and an orthoconical subsidence area, connecting at the rotation point. The damage model captures the progressive failure process and potential evolution path of the suction cylinder foundation under liquefied site conditions, providing deeper insight into the foundation's overturning resistance and failure mechanisms.

Acknowledgments

This research is supported by the National Science Foundation for Distinguished Young Scholars of China (Grant No.52225807).

References

1. Liu, Z., Lu, Z., Wang, Z., et al. (2024) Offshore wind power development potential and economic analysis of transmission. *Renewable Energy*, 42(11): 1498–1503. DOI:10.13941/j.cnki.21-1469/tk.2024.11.009.
2. Wang, Y., Zhou, X., Yang, L., et al. (2024) Development status and trend of wind turbine support structure technology. *Steel Structures*, 39(10): 1–13. DOI:10.13206/j.gjgS24070220.
3. Changka, W., Kunpeng, W. (2021) Fatigue characteristics of catenary wind turbine structures under combined wind and wave. *Renewable Energy*, 39(12): 1617–1622. DOI:10.13941/j.cnki.21-1469/tk.2021.12.021.

4. Yang, C., Zhang, J., Wang, R. (2017) Seismic analysis of offshore wind power suction bucket foundation. *Journal of Tsinghua University (Natural Science Edition)*, 57(11): 1207–1211. DOI:10.16511/j.cnki.qhdxxb.2017.26.063.
5. Yuan, M.-H. (2023) Study on bearing characteristics of suction bucket foundation in saturated soft clay under cyclic wind and wave loading. *Qingdao University of Technology*. DOI:10.27263/d.cnki.gqudc.2023.000705.
6. Sun, X., Luan, M., Tang, X. (2010) Study on horizontal bearing capacity of barrel-shaped foundation in saturated soft clay foundation. *Geotechnics*, 31(2): 667–672. DOI:10.16285/j.rsm.2010.02.037.
7. Cheng, X., Lu, J., Zhuang, Q., et al. (2022) Lateral cyclic behavior of OWT tripod suction bucket foundation in clays. *Ocean Engineering*. DOI:10.1016/j.oceaneng.2022.112635.
8. Luo, L., Wang, Y., Huang, J., et al. (2021) Study on the effect of ocean cyclic loading on the horizontal bearing capacity of suction drum foundation. *Journal of Solar Energy*, 42(3): 142–147. DOI:10.19912/j.0254-0096.tynxb.2020-0011.
9. Li, C., Wang, J., Liu, Z. (2005) Study on cyclic bearing capacity of single-barrel foundation for soft ground. *Journal of Geotechnical Engineering*, (9): 1040–1044.
10. Jiao, B., Shi, Z., Lu, X., et al. (2010) Centrifuge experimental study on the horizontal dynamic load response of barrel-shaped foundation in pulverized ground. *Engineering Mechanics*, 27(7): 131–141.
11. Lu, X., Wang, Y., Zhang, J., et al. (2005) Centrifuge experimental study on the deformation of barrel-shaped foundation under horizontal dynamic load. *Journal of Geotechnical Engineering*, (7): 789–791.
12. Jeong, Y. H., Kim, J. H., Manandhar, S., et al. (2019) Centrifuge modelling of drained pullout and compression cyclic behaviour of suction bucket. *International Journal of Physical Modelling in Geotechnics*, 20(2): 1–30. DOI:10.1680/jphmg.18.00044.
13. Lian, J., Zhao, Y., Dong, X., et al. (2021) An experimental investigation on long-term performance of the wide-shallow bucket foundation model for offshore wind turbine in saturated sand. *Ocean Engineering*, 228: 108921.
14. Zhu, B., Ying, P., Guo, J., et al. (2013) Bearing capacity analysis and design of suction barrel foundation for offshore wind turbines. *Journal of Geotechnical Engineering*, 35(S1): 443–450.
15. Achmus, M., Akdag, C. T., Thieken, K. (2013) Load-bearing behavior of suction bucket foundations in sand. *Applied Ocean Research*, 43(5): 157–165. DOI:10.1016/j.apor.2013.09.001.
16. Chengshun, X., Chong, Y., Xiuli, D., et al. (2024) Experimental study on the influence of cyclic loading frequency on liquefaction characteristics of saturated sand. *Géotechnique*, (1-14).
17. Chong, Y., Ke, L., Chengshun, X., et al. (2023) Experimental study on cyclic deformation properties of saturated Fujian sand at different loading frequencies. *Underground Space*, 13150–165.
18. Kuo, Y. S., Chong, K. J., Tseng, Y. H., et al. (2024) Excess pore water pressure response of soil inside the mini bucket embedded in saturated soil under seismic loading. *Soil Dynamics and Earthquake Engineering*, 182. DOI:10.1016/j.soildyn.2024.108751.
19. Zhang, P., Xiong, K., Ding, H., et al. (2014) Anti-liquefaction characteristics of composite bucket foundations for offshore wind turbines. *Journal of Renewable and Sustainable Energy*, 6(5). DOI:10.1063/1.4895909.
20. Hussein, A. F., El Nagggar, M. H. (2022) Seismic behaviour of piles in non-liquefiable and liquefiable soil. *Bulletin of Earthquake Engineering*, (1): 20. DOI:10.1007/s10518-021-01244-4.

21. Cuéllar, P. (2011) Pile foundations for offshore wind turbines: numerical and experimental investigations on the behaviour under short-term and long-term cyclic loading.
22. Naggar, M. H. E., Bentley, K. J. (2000) Dynamic analysis for laterally loaded piles and dynamic p-y curves. *Canadian Geotechnical Journal*, 37(6): 1166–1183.
23. Lin, S. S., Liao, J. C. (1999) Permanent strains of piles in sand due to cyclic lateral loads. *Journal of Geotechnical & Geoenvironmental Engineering*, 125(9): 798–802. DOI:10.1061/(ASCE)1090-0241(1999)125:9(798).
24. Li, D., Zhang, J., Zhang, Y., et al. (2021) Horizontal cyclic characteristics and cumulative turning angle change rule of skirt suction foundation in saturated sandy soil. *Geotechnics*, 42(3): 611–619. DOI:10.16285/j.rsm.2020.1296.
25. Chong, S. (2017) Numerical simulation of offshore foundations subjected to repetitive loads. *Ocean Engineering*, 142: 470–477.
26. Chong, S., Pasten, C. (2018) Numerical study on long-term monopile foundation response. *Marine Georesources & Geotechnology*, 36(2): 190–196.
27. Wang, X., Ma, C., Li, J. (2021) Experimental and simulation study on the dynamic response of offshore wind turbine cylinder foundation-site. *Journal of Tianjin University (Natural Science and Engineering Technology)*, 54(8): 790–798.

Open Access This chapter is licensed under the terms of the Creative Commons Attribution-NonCommercial 4.0 International License (<http://creativecommons.org/licenses/by-nc/4.0/>), which permits any noncommercial use, sharing, adaptation, distribution and reproduction in any medium or format, as long as you give appropriate credit to the original author(s) and the source, provide a link to the Creative Commons license and indicate if changes were made.

The images or other third party material in this chapter are included in the chapter's Creative Commons license, unless indicated otherwise in a credit line to the material. If material is not included in the chapter's Creative Commons license and your intended use is not permitted by statutory regulation or exceeds the permitted use, you will need to obtain permission directly from the copyright holder.

